Article Identifier
DOI: 10.22032/dbt.58877
URN: urn:nbn:de:gbv:ilm1-2023isc-088:9

60th ILMENAU SCIENTIFIC COLLOQUIUM
Technische Universität Ilmenau, 4 – 8 September 2023
URN: urn:nbn:de:gbv:ilm1-2023isc:1

CONTROL FOR NON-LINEAR COMPLIANT ACTUATION OF AN UPPER ARM EXOSKELETON

Max Jäger, Thomas Helbig and Hartmut Witte

Technische Universität Ilmenau, Department of Mechanical Engineering,
Biomechatronics Group, Ilmenau, Germany

ABSTRACT

Musculoskeletal diseases of the back and upper extremities are one of the main causes of sick leave in Europe. Exoskeletons are one possible approach to preventive measures. The Biomechatronics Group at Technische Universität Ilmenau is developing an antagonistically actuated exoskeleton with non-linear compliance to support flexion and extension of the elbow in repetitive tasks like in assembly. Here, we present a control strategy to achieve joint stiffness control while benefitting from the advantages of non-linear compliant actuation. We use a decentralized control approach, combining two PID controllers to control joint position and string force and thus, joint stiffness, in the antagonistically acting drive. We show limitations and benefits of this approach through simulation and measurement.

Index Terms - exoskeleton, control, non-linear compliance, antagonistic actuators

1. INTRODUCTION

The use of powered exoskeletons in workplaces that are intensive in manual labor has become more and more attractive in the recent years. In contrast to powered exoskeletons used in medical applications such es rehabilitation or restauration, such devices can be used to lighten the load of the workers' tasks to reduce the risk of developing musculoskeletal diseases. This application is especially interesting because musculoskeletal diseases are among the major reasons for sick leave and long-term physical impairments [1].
With this goal of prevention, the group of Biomechatronics of Technische Universität Ilmenau joined the research project LEVIAKTOR ("LEVItation mittels AKTorik in ORthesen"; English: levitation via actuators in orthoses, BMBF 16SV8004, 2018-2021) to develop a powered exoskeleton for industrial use. The exoskeleton aimed to reduce the load on the worker to delay and reduce muscular fatigue. This should lead to a reduced risk of musculoskeletal diseases [2]. During the project LEVIAKTOR, the testbed exoskeleton AMULETT (Active MUscle controlled Lightweight ExoskeleTon Testbed) was developed to test sensors, actuation principles and controlled schemes (system description in [3]). The exoskeleton attaches to the users arm to support flexion and extension of the elbow. It uses antagonistic actuators ("biceps" and "triceps"), corresponding to the biological model, connected to the exoskeleton via strings. In each string, a non-linear compliant element is integrated. Compliant elements with non-linear characteristics are needed to enable variable joint stiffness and safe operation of the antagonistically acting motors [4].
Using compliant elements with non-linear characteristics increases the complexity of control. During operation, both strings have to remain under tension in order to achieve controlled

behavior when facing disturbances like external forces. Controlling the tension in the antagonistically acting string during motion allows biomimetic behavior regarding joint stiffness: At the beginning of motion, the tension of the antagonist is reduced to allow fast acceleration of the joint according to the agonist's movement. When nearing the target position, the antagonist is tensioned again, to increase joint stiffness and allow for more precise joint positioning [5, 6].

1.1 Control of joint position and stiffness

In recent years, various approaches have been explored to develop rehabilitation exoskeletons and robotic hand systems with efficient control mechanisms. This literature review highlights key findings from several relevant studies in this field.

Li et al. [7] proposed a rehabilitation exoskeleton that utilizes cable-driven joints. The control architecture consisted of a two-level approach. At the high level, a computed torque method (CTM) controller determined the required cable tensions to achieve desired joint positions and stiffness. The low-level control involved a combination of proportional-integral-derivative (PID) control, feed-forward control, and motor friction compensation to drive the motors based on the cable tensions provided by the high-level controller. Huang et al. [8] presented two distinct approaches for controlling antagonistic actuation in a four-bar linkage system with nonlinear elastic elements. In the first approach, an "optimal control" strategy was employed, assuming direct and independent control of joint torque and stiffness. The second approach focused on minimizing the motions by moving the motors the shortest distance necessary to achieve the target joint torque and stiffness, using proportional-derivative (PD) controllers for motor control. Fasel et al. [9] proposed a tendon-controlled endoscope tip system with cascaded control. The inner loop employed a PD controller to regulate tendon forces, while the outer loop utilized a proportional controller for position control. The proportional controller estimated the endoscope tip angle using forward kinematics of the system based on the tendon positions as feedback. Tendon forces were estimated through the deflection of linear springs. Tonietti et al. [10] presented an approach involving a PD controller to achieve position and stiffness control in a system with two motors acting on a toothed belt. The control strategy entailed changing the co-rotating and counter-rotating movements of the motors. Lenzi et al. [11] investigated the independent control of stiffness and position using hydraulic actuators and nonlinear compliant elements for their NEURARM platform. Their control architecture combined model-based feed-forward control at the high level with closed-loop control at the low level. Stevens [12] focused on antagonistic shape memory alloy (SMA) actuators and proposed an artificial neural network (ANN) control strategy for achieving effective actuation. Muralidharan et al. [13] proposed a model-based feed-forward control approach for antagonistically actuated X-bar linkages, although further details regarding the control mechanism were not provided in this paper.

1.2 Our contribution

In this paper, we propose a control scheme for AMULETT to improve upon our previous investigations of the system [3] and allow the use of a biomimetic stiffness profile. The proposed control also allows to switch which drive acts as the agonist to enable the exoskeleton to support the user in both flexion and extension motions.
We investigate the proposed control scheme both in simulation and in experiments to test the following hypotheses:

1. Controlling the string tension has positive effects on position control: Rise time and position error are reduced,

2. Stiffness control allows for more biomimetic behavior: Joint stiffness is variable and controlled during motion, depending on the difference between desired and actual joint position [5, 6],
3. The proposed control allows for smooth switching of the agonistically acting drive: The switch does not negatively impact position control performance.

2. MATERIALS AND METHODS

2.1 System description

To investigate the proposed control scheme, the AMULETT exoskeleton is simplified and stripped of all unneeded parts, namely the cuffs and the dummy arm (see [3]). The remaining structure, consisting of the supporting beams for upper and forearm, connected by a ball bearing joint, is fixed to a table. The structure is oriented such that the forearm supporting beam swings horizontally to reduce the influence of gravity on the experiment. The experimental setup can be seen in Figure 1.

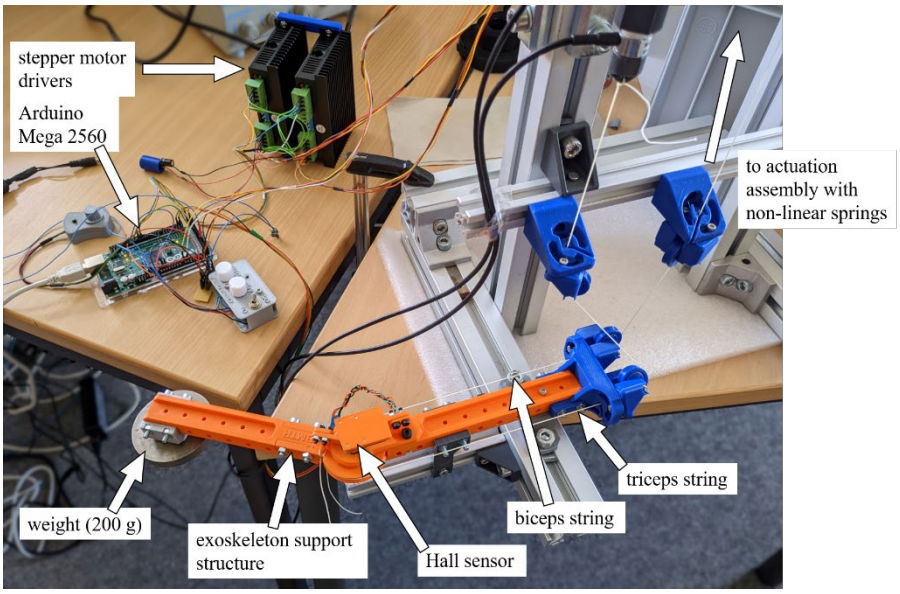

Figure 1: Experimental setup used for the measurements presented in this paper.

To describe the system using a differential equation for simulation, we assume that all masses are point masses acting solely on their respective centers of mass. With these simplifications, the system can be described using the following equations (1) to (5) and Figure 2.

$$\ddot{x_a} - \frac{f(\Delta l_1)}{J} \cdot R_2 + \frac{M_m}{J} \cdot sin(x_a) + 2\delta \cdot \dot{x_a} + \frac{f(\Delta l2)}{J} \cdot R_2 = 0 \qquad (1)$$

Where

$$M_m = g \cdot \sum_{i=1}^{N} m_i \cdot l_i \quad (2)$$

$$J = \frac{1}{12} \sum_{i=1}^{N} m_i \cdot (\max_{1 \le i \le N} l_i)^2 + \sum_{i=1}^{N} m_i l_i^2 \quad (3)$$

$$\Delta l_1 = x_{e1} \cdot R_1 - x_a \cdot R_2 \quad (4)$$

$$\Delta l_2 = x_a \cdot R_2 - x_{e2} \cdot R_1 \quad (5)$$

With

J	Inertia, according to the Huygens-Steiner theorem, assuming the mass is distributed in a thin rod
M_m	Torque due to static forces (weight)
Δl_1, Δl_2	Deflection of spring 1 resp. 2
R_1	Radius of the drive pulley
R_2	Radius of the exoskeleton pulley
δ	Decay rate, experimentally determined
$f(\cdot)$	Force of the non-linear spring assembly as a function of its deflection
m_i, l_i	Masses and their corresponding lever arms with respect to the exoskeleton's joint
g	Gravitational constant
x_{e1}, x_{e2}	Angle of the biceps resp. triceps motor
x_a	Angle of the exoskeleton joint

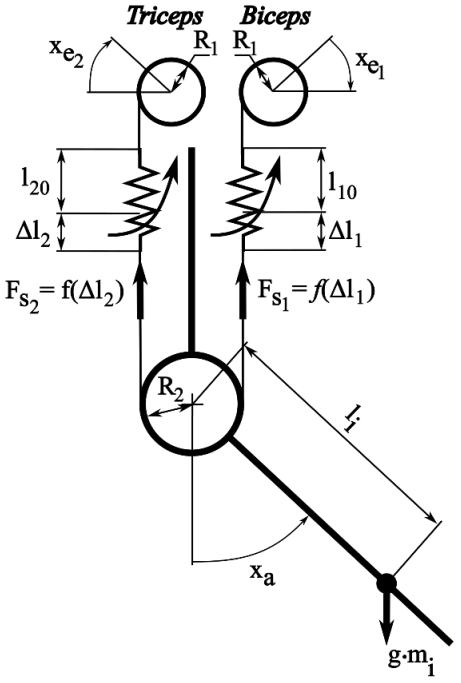

Figure 2: Sketch of the simplified support structure with actuation. All symbols are explained below.

The system is modelled in Matlab® Simulink® (Matlab® R2021b, The Mathworks, Inc). The force-deflection curve of the non-linear springs is calculated and inserted into the Simulink model using a look-up table.
Previous experiments have shown that the decay rate δ depends on the preload force of the antagonistic drive due to friction in the system also being preload dependent. To determine this dependency, the decay rate of manually excited oscillations was determined in a separate experiment. For the experiment, a weight of 200 g was attached to the exoskeleton's forearm support beam at 143 mm from the joint to increase inertia. Moving the exoskeleton arm without load also deviates greatly from its later application on the human arm. The decay rate vs preload force data and a fit using an exponential function can be seen in Figure 3. The decay rate was then inserted into the Simulink model using the fit function, limiting the minimum damping to zero to avoid a negative decay rate.

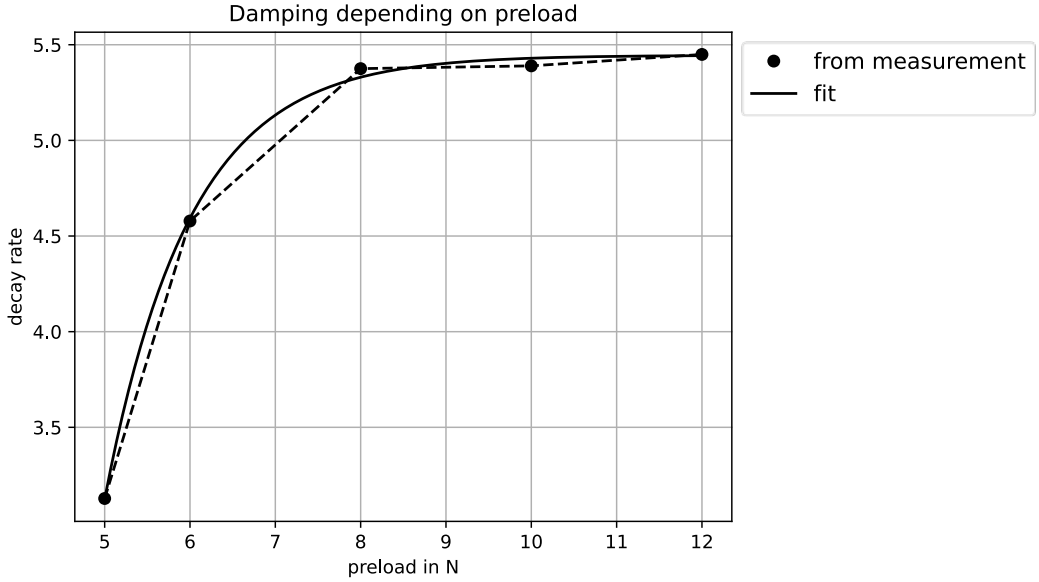

Figure 3: Preload-dependent damping of the system. An exponential function of the form $a \cdot e^{(bx+c)}+d$ was used for regression. Parameters: a = -1.79094945, b = -1.00214543, c = -5.25850838, d = 5.44504523.

2.2 Control

To control the exoskeleton's joint position and stiffness by means of antagonistic drives, we propose a decentralized control approach. One PID controller each is implemented to control the joint's position and antagonistic string tension separately, according to the block diagram in Figure 4.

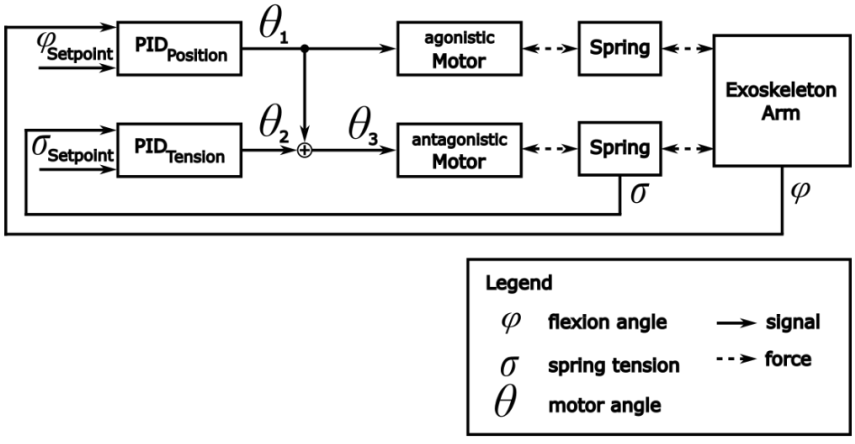

Figure 4: Block diagram of the proposed control approach.

While both motors influence the joint position, only the *agonistic* motor is controlled directly by the position controller. The *antagonistic* motor's position is controlled by the sum of the position and string tension controllers' outputs. For feedback, the position controller uses the angle of the exoskeleton's joint. The string tension controller uses an estimate of the string force as feedback which is calculated by measuring the deflection of the linear springs in the non-linear spring assembly (see Figure 5 (a)) and putting it through a look-up table of the non-linear spring's characteristic. Figure 5 (b) shows a comparison between string force measured with a strain gauge sensor and the estimated force using the mathematical model described in [3] and spring deflection measurements using a sliding potentiometer.

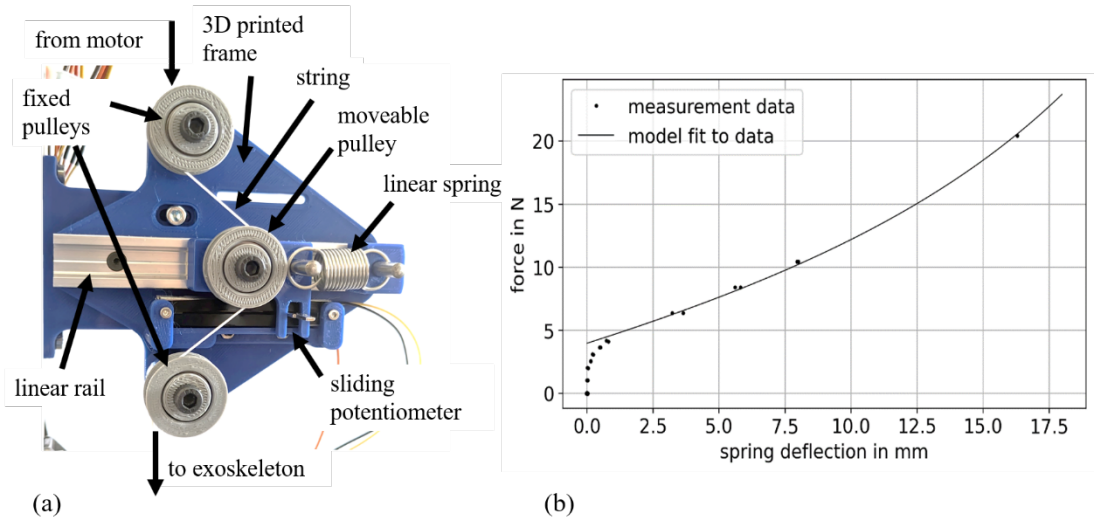

Figure 5: (a) Non-linear spring assembly used in the experimental setup. (b) Comparison between measured force data and force estimated using a mathematical model of the non-linear spring. Because of the increasing error at low forces, only force estimations above 5 N were used in the final implementation.

Which drive acts as the agonist is determined by comparing the deflection of the linear springs in the non-linear spring assemblies in both strings: The agonist is the drive which contributes more force to the motion [14]. If both springs are deflected equally, the direction of the desired motion determines the agonistically acting drive. Since the agonist switches, simply adding the tension controller's output to the antagonist's position signal allows for a smooth transition by means of an offset that's recalculated at every switch and added to the position signal of each motor. The offset ensures, that the new agonistic drive's position is equal to its position before the switch. This way, discontinuities of the drives' position signals are avoided.
For the measurements using the physical AMULETT system, the proposed control was implemented entirely on an Arduino microcontroller (Arduino Mega 2560, Arduino). The exoskeleton's elbow angle is measured by means of a Hall-effect based sensor (AS5048B; ams-OSRAM AG, Premstaetten, Austria) on the exoskeleton's joint. The deflections of both linear springs are measured using linear sliding potentiometers (10 kΩ, WMYCONGCONG).

We compare the following control configurations, each both in simulation and measurement:

- Only position control,
- Position and string tension control,
  - With force setpoint 5 N,
  - With force setpoint 10 N,
  - With variable joint stiffness.

Variable joint stiffness was achieved by scaling the desired string force by a factor depending on the position error (see equation (6) and Figure 6). This ensures low stiffness when the position error is large (at the beginning of motion) and increasing stiffness when nearing the desired position.

$$f_\sigma = \frac{\left(1 - (\sigma_{min}/\sigma)\right)}{d_{offset}^4} \cdot \left|\varphi_{Setpoint} - \varphi\right|^4 + \frac{\sigma_{min}}{\sigma} \qquad (6)$$

With

f_σ	String tension scaling factor
σ	Desired string tension
σ_{min}	Minimum desired string tension
d_{offset}	Error between position setpoint and actual position at which f_σ is minimal
$\varphi_{Setpoint}$	Desired position
φ	Actual position

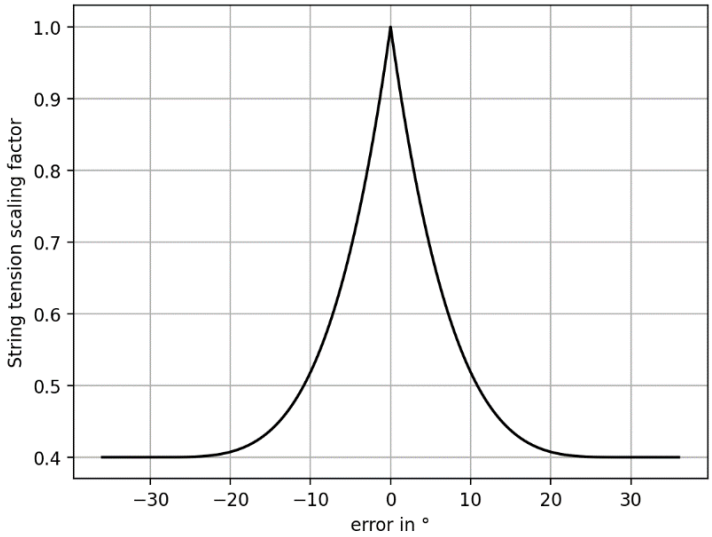

Figure 6: String tension scaling factor used for variable stiffness experiments. The curve was calculated using equation (6) with parameters σ = 10, σ_{min} = 4, d_{offset} = 30°.

The parameters of the PID controllers were determined empirically. Methods described by (Ziegler and Nichols, 1942) [15] and (Chien et al., 1952) [16] were used to obtain initial parameters from which manual adjustments were made to improve performance. For the physical AMULETT system, the parameters of the position controller needed to be different with and without the string tension controller. To maintain string tension without the string tension controller, an offset of 20° was added to both drives' signals, both in simulation and in the physical system to maintain comparability. See Table 1 for the parameters used in simulations and measurements.

To evaluate and compare the control configurations' performances, we chose the following measures on the system's step responses: The integrated squared error (ISE) (Eq. (7)), the integrated absolute value of the derivative of the drives' position signals (integrated absolute angular velocity, ISAV) (Eq. (8)) to estimate required power to achieve the desired performance and the rise time. The ISE is calculated for both the joint position signal and the string force signal. Rise time was calculated as the time difference between the step in the setpoint signal and the moment when the position or string force signal reached an error margin

around the setpoint. For the position signal, this margin was ±2°, according to [17]. For string force, we chose an error margin of ±5% of the setpoint force. This rather liberal error margin was chosen because of the inherent elasticity of our experimental setup due to 3D printed parts, which reduces the accuracy one can expect from a length measurement-based force estimation. The evaluation measures were applied to the system's response to steps from 0° to 45° of the position setpoint for one simulation run for each configuration and for ten repetitions of the step input for the physical AMULETT system. Because the system should behave symmetrically for flexion and extension, we only evaluate flexion motion.

Table 1: PID tuning parameters.

Simulation	Only position control	Kp_P	20
		Ki_P	22.5
		Kd_P	0.75
	Position control and string tension control	Kp_P	20
		Ki_P	22.5
		Kd_P	0.75
		Kp_T	19.5
		Ki_T	25
		Kd_T	0.5
Measurements with AMULETT	Only position control	Kp_P	0.095
		Ki_P	5.94
		Kd_P	0.02
	Position control and string tension control	Kp_P	0.11
		Ki_P	5.8
		Kd_P	0.0137
		Kp_T	4.8
		Ki_T	90
		Kd_T	0.1

$$ISE = \int_0^T \text{error}^2 \, \text{dt} \qquad (7)$$

$$ISAV = \int_0^T \omega^2 dt \qquad (8)$$

With

error	Difference between the setpoint and the actual value
T	Measurement time
ω	Rate of change of the drive's position signal

3. RESULTS

3.1 Position control performance

In the simulations, the rise time remains practically the same with and without the proposed control approach. In the measurements however, the rise time increases. With a tension setpoint of 5 N, the average increase is 0.75 s, with 10 N, it's 0.1 s. The average rise times for the different configurations can be seen in Table 2.

Table 2: Rise time for different control configurations.

Simulation / Measurement	Tension control	Variable stiffness	Rise time
Simulation			0.26
Simulation	x (5 N)		0.25
Simulation	x (10 N)		0.25
Simulation	x	x	0.24
Measurement			1.09
Measurement	x (5 N)		1.84
Measurement	x (10 N)		1.19
Measurement	x	x	2.43

For position control, the proposed control approach increases the ISE, as can be seen in Table 3. This effect is much more prominent in the measurements (maximum increase 12.3%) as compared to the simulation results (maximum increase 2.9%). The increase is also bigger for measurements with a higher string force setpoint (12.3% vs. 1.5%). For simulations, the ISE increases more with a lower string force setpoint (2.9% vs. 0.77%).

Table 3: Integral of the squared position error for different control configurations.

Simulation / Measurement	Tension control	Variable stiffness	ISE (position)
Simulation			116.21
Simulation	x (5 N)		119.58
Simulation	x (10 N)		117.11
Simulation	x	x	115.12
Measurement			579.23
Measurement	x (5 N)		588
Measurement	x (10 N)		650.57
Measurement	x	x	585.07

3.2 Tension control performance

For tension control, the ISE decreases when using our control system (see Table 4). Here, the reduction is more pronounced in the simulation results. For a force setpoint of 10 N, the tension ISE is reduced by 98.7%.

Figure 7 shows an example of the measured force signal during the first three steps in the position setpoint signal. Without tension control, the string force varies throughout the course of the measurement.

Table 4: Integral of the squared tension error for different control configurations.

Simulation / Measurement	Tension control	Variable stiffness	ISE (tension)
Simulation			11.17
Simulation	x (5 N)		7.82
Simulation	x (10 N)		0.15
Simulation	x	x	5.45
Measurement			0.98
Measurement	x (5 N)		0.2
Measurement	x (10 N)		0.5
Measurement	x	x	2.03

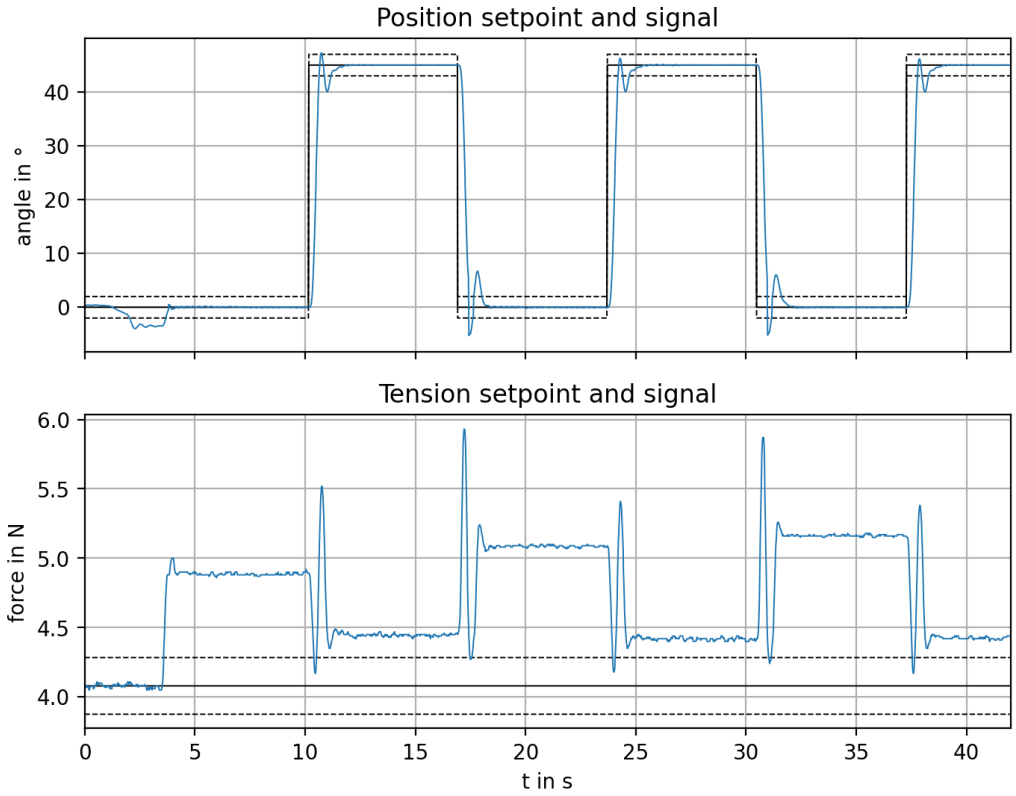

Figure 7: The first three step responses without tension control. Black solid lines: Setpoint signals. Black dashed lines: error margin around the setpoints (2° for position, 5% of the setpoint for force control). Blue lines: position and force signals. The average of the force signal in the first two seconds was set as the force setpoint.

3.3 Integrated squared angular velocity

We compare the ISAV separately for the biceps and triceps drives (see Table 5). For the measurements, the change of ISAV values compared to the configuration without tension control is not consistent. With tension control and a force setpoint of 5 N, the ISAV for the biceps decreases slightly while it increases for the triceps. For 10 N, the biceps' ISAV increases by a factor of 2.64 and the triceps' ISAV by 1.2, compared to the values without tension control. The simulations however show a decrease with the proposed control system for both the biceps (relative decrease > 62%) and the triceps drive's signal (relative decrease > 10%). This is consistent for all three control configurations with tension control.

Table 5: Integral of the squared angular velocities of biceps and triceps drives for different control configurations.

Simulation / Measurement	Tension control	Variable stiffness	ISAV (biceps)	ISAV (triceps)
Simulation			89042.2	1.25141e+08
Simulation	x (5 N)		33263.4	1.12419e+08
Simulation	x (10 N)		901.25	9.7497e+07
Simulation	x	x	36866.3	9.92114e+07
Measurement			18.61	5998.15
Measurement	x (5 N)		17.22	6485.63
Measurement	x (10 N)		49.14	7237.26
Measurement	x	x	197.06	5726.74

3.4 Variable joint stiffness

Simulations with variable joint stiffness showed a slight decrease in rise time and position ISE, when compared to the other control configurations. It performed comparably to configurations with tension control regarding tension ISE and ISAV values.

Figure 8 (a) shows the string force setpoint and estimation signal for a simulation with variable string force setpoint, resulting in varying joint stiffness.

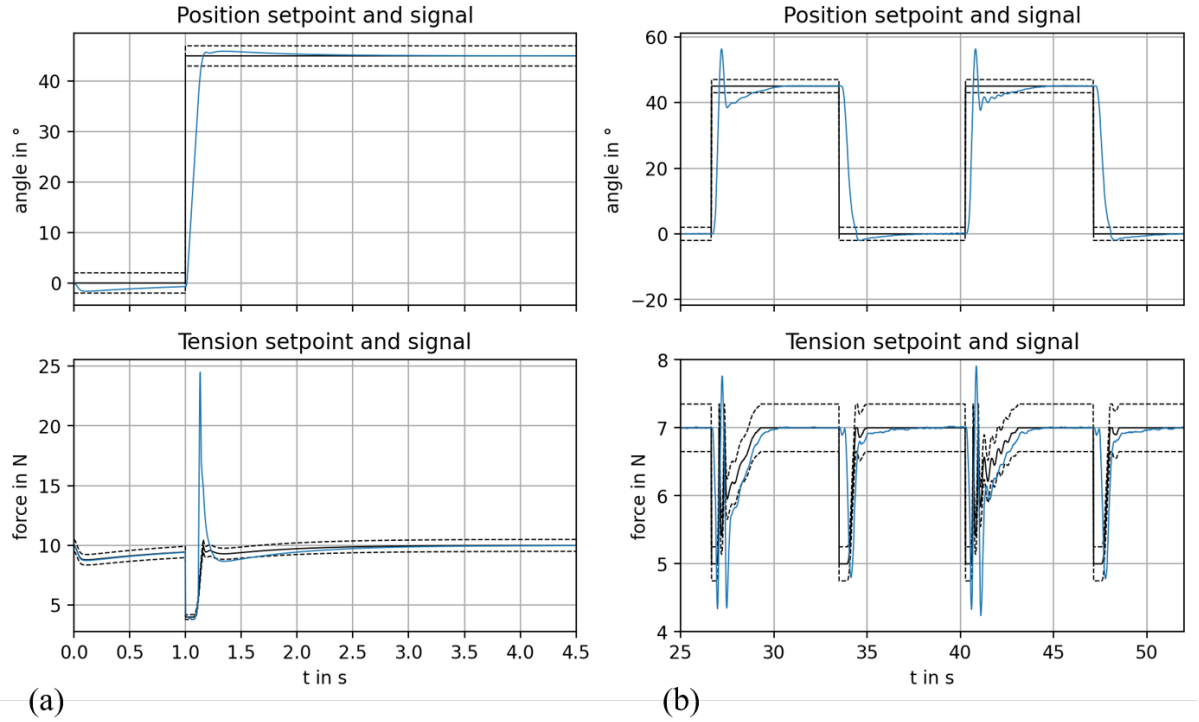

Figure 8: Step response with variable joint stiffness, depending on the position error. (a) Simulation. (b) Measurement. Black solid lines: setpoint signals. Black dashed lines: error margin around the setpoints (2° for position, 5% of the setpoint for force control). Blue: system response.

Measurements with variable stiffness showed an increase in rise time and tension ISE, which appeared due to larger overshoot. Position ISE showed an average value comparable to the

configurations without tension control and with tension control and a force setpoint of 5 N. Biceps ISAV showed a large increase, while triceps ISAV showed the lowest value of all compared configurations. Figure 8 (b) shows the position and force signals of a measurement with variable string force setpoint. Note the oscillation after the step in the position signal.

3.5 Switching the agonist

Figure 9 shows the position and force signals for movements with enabled switching of the agonistically acting drive. The position signal shows no visible peaks indicating that the alternating agonist would have a negative effect. However, the force signal shows discontinuities when switching. Note also the oscillatory behavior of the force signal.

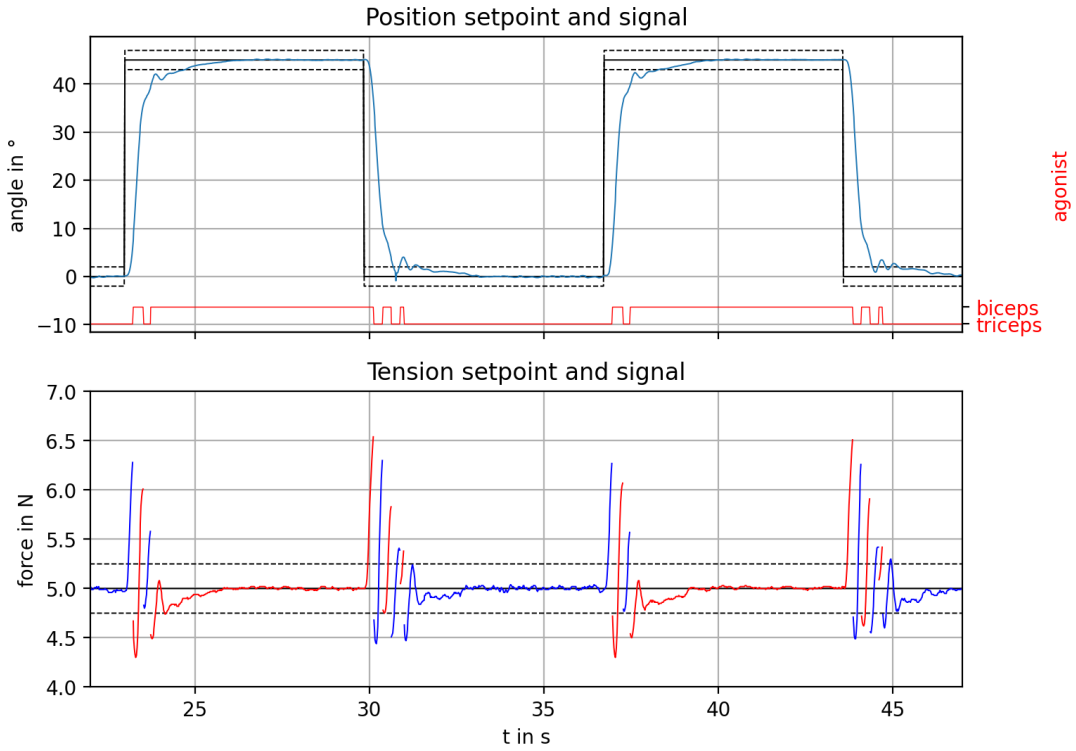

Figure 9: Example step responses with tension control and switching agonist. In the lower plot, the force signal used as feedback for the tension controller switches between biceps (blue) and triceps (red) force signal. Black solid lines: Setpoint signals. Black dashed lines: error margin around the setpoints (2° for position, 5% of the setpoint for force control).

4. DISCUSSION

Control performance depends heavily on the PID controllers' parameters. Thus, comparability between measurements with and without string tension control and between measurements and simulation is limited. We will focus on the simulations first, since the position controller could be used with the same parameters, with and without tension control.

The addition of tension control has a minor negative effect on position control. Rise time is reduced slightly, position ISE is increased slightly. The cause for the increased position ISE is most likely the fact that, due to the decentralized structure of the proposed control system, both controllers act as a disturbance for each other. However, the negative effects are comparatively small and can be considered negligible. On the other hand, ISAV for both the biceps and triceps

drives is reduced, meaning the required energy to achieve a comparable position step response was decreased. The effect is more prominent in the biceps' ISAV.
As one would expect, adding tension control reduces the tension ISE. Especially with a higher tension setpoint, tension ISE was greatly decreased. The cause for this is likely the non-linear characteristic of the springs in combination with the string tension dependent damping of the system (see Section 2.1). It is worth noting, that the simulation does not incorporate mass or inertia of the non-linear spring, which makes the simulated spring much more responsive to control influences than its physical representation.
When changing the tension controller's setpoint depending on the position error, the simulated system behaves comparably to the configurations without variable joint stiffness. Changing the joint stiffness dynamically is performed without any prominent changes in system behavior.
In our measurements, the added tension controller only leads to negligible improvements. The results are comparable or slightly worse than without tension control. When comparing controller gains (see Table 1), the difference between simulation and a "real" setup become obvious. Due to noisy sensor data, the controller gains cannot be set as high in the experimental setup as in the simulation without making the system unstable, which leads to higher rise times, but also much lower ISAV values, when compared to simulation.
Measurements show that the system's dynamics change substantially with variable joint stiffness. Overshoot in the position signal followed by slight oscillations imply that the position controller gains have to be set differently with and without variable joint stiffness. The reduction in position control performance can be attributed to this.
Tension feedback enables switching between supported flexion and extension movements. Switching has only minor effects on the performance of position control. However, the smoothness of the force signal used as input for tension control should be improved. The visible oscillations are likely a result of the controller's tuning, which should be adapted to accommodate for the future use of both variable joint stiffness and switching of the agonistically acting drive.
While simulation is useful to determine general feasibility of control approaches, real world application and its errors make experimental setup necessary to acquire data on the suitability of a control approach. This holds especially true when components are 3D printed and low-cost.
In our evaluation of the proposed control approach, we used evaluation measures to quantify the systems behavior in order to improve comparability between control configurations. The different approaches in literature (see Section 1.1) only present qualitative evaluation of their control approaches, mainly because control is not the main objective of these publications.

5. CONCLUSION AND OUTLOOK

5.1 Conclusion

We present a control approach to implement string tension control in an antagonistically actuated, light-weight, low-cost exoskeleton testbed. This allows for controlled, adjustable joint stiffness, independent of joint position. The string force feedback can be used to implement variable joint stiffness to mimic biological joint stiffness behavior during motion. It also allows for switching of the agonistically acting drive to support both flexion and extension movements.
Our results don't support hypothesis 1: Neither the simulation results nor the measurements exhibit reduced rise time or position ISE with the added tension controller. However, negative effects were negligible in simulations. Based on the presented results and with the prospect of future improvements on the proposed control approach, we don't see hypotheses 2 or 3 falsified.

5.2 Outlook

Building on the proposed control approach, we intend to investigate and improve its behavior in the “real” exoskeleton testbed setup. Especially its interaction with Bowden cables, which introduce a higher preload-dependent friction and thus damping of the system, will be investigated. The proposed approach can also be used to implement joint torque control with low-cost components. To evaluate the quality of this control approach in an actual exoskeleton application, we plan to test the system on a human arm, using interaction forces as feedback to control the exoskeletons motion.

ACKNOWLEDGEMENT

ChatGPT (GPT-3, OpenAI’s large-scale language-generation model) has been used to generate some of the text and to improve the writing style of this paper. The authors reviewed, edited, and revised the ChatGPT generated texts to their own liking and take ultimate responsibility for the content of this publication.

REFERENCES

[1] EU-OSHA, *Work-related musculoskeletal disorders: prevalence, costs and demographics in the EU.* [Online]. Available: https://osha.europa.eu/en/publications/msds-facts-and-figures-overview-prevalence-costs-and-demographics-msds-europe (accessed: Jan. 26 2023).

[2] T. Helbig, S. Kreipe, M. Goos, S. Wenzel, N.-P. Schumann, and H. Witte, “Prediction of movement for adaptive control of an upper limb exoskeleton,” *The 9.5th international symposium on Adaptive Motion of Animals and Machines. Ottawa, Canada (Virtual Platform). 2021-06-22/25. Adaptive Motion of Animals and Machines Organizing Committee.*, 2021. [Online]. Available: https://ir.library.osaka-u.ac.jp/

[3] M. Jäger, T. Helbig, M. Goos, S. Köhring, and H. Witte, “Characterization of an Antagonistic Actuation System with Nonlinear Compliance for an Upper-Arm Exoskeleton,” *Actuators*, vol. 12, no. 5, p. 196, 2023, doi: 10.3390/act12050196.

[4] K. Koganezawa, T. Nakazawa, and T. Inaba, “Antagonistic control of multi-DOF joint by using the actuator with non-linear elasticity,” in *Proceedings 2006 IEEE International Conference on Robotics and Automation, 2006. ICRA 2006*, Orlando, FL, USA, 2006, pp. 2201–2207.

[5] N. Hogan, “Adaptive control of mechanical impedance by coactivation of antagonist muscles,” *IEEE Trans. Automat. Contr.*, vol. 29, no. 8, pp. 681–690, 1984, doi: 10.1109/TAC.1984.1103644.

[6] P. L. Gribble, L. I. Mullin, N. Cothros, and A. Mattar, “Role of cocontraction in arm movement accuracy,” *Journal of neurophysiology*, vol. 89, no. 5, pp. 2396–2405, 2003, doi: 10.1152/jn.01020.2002.

[7] Z. Li *et al.,* “Mechatronics design and testing of a cable-driven upper limb rehabilitation exoskeleton with variable stiffness,” *The Review of scientific instruments*, vol. 92, no. 2, p. 24101, 2021, doi: 10.1063/5.0037317.

[8] T.-H. Huang, H.-P. Huang, and J.-Y. Kuan, “Mechanism and Control of Continuous-State Coupled Elastic Actuation,” *J Intell Robot Syst*, vol. 74, 3-4, pp. 571–587, 2014, doi: 10.1007/s10846-013-9937-0.

[9] L. Fasel, N. Gerig, P. C. Cattin, and G. Rauter, “Control Evaluation of Antagonistic Series Elastic Actuation for a Robotic Endoscope Joint,” *J Bionic Eng*, vol. 19, no. 4, pp. 965–974, 2022, doi: 10.1007/s42235-022-00180-6.
[10] G. Tonietti, R. Schiavi, and A. Bicchi, “Design and Control of a Variable Stiffness Actuator for Safe and Fast Physical Human/Robot Interaction,” in *Proceedings of the 2005 IEEE International Conference on Robotics and Automation*, Barcelona, Spain, 2005, pp. 526–531.
[11] T. Lenzi, N. Vitiello, J. McIntyre, S. Roccella, and M. C. Carrozza, “A robotic model to investigate human motor control,” *Biological cybernetics*, vol. 105, no. 1, pp. 1–19, 2011, doi: 10.1007/s00422-011-0444-8.
[12] J. M. Stevens, “Actuation and Control Strategies for Miniature Surgical Robotic Systems,” Master thesis, North Carolina State University, Raleigh, North Carolina, USA, 2002. [Online]. Available: https://repository.lib.ncsu.edu/handle/1840.16/1753
[13] V. Muralidharan, N. Testard, C. Chevallereau, A. Abourachid, and P. Wenger, “Variable Stiffness and Antagonist Actuation for Cable-Driven Manipulators Inspired by the Bird Neck,” *Journal of Mechanisms and Robotics*, vol. 15, no. 3, 2023, doi: 10.1115/1.4062302.
[14] K. S. Saladin, *Human anatomy,* 3rd ed. New York, NY: McGraw-Hill Higher Education, 2011.
[15] J. G. Ziegler and N. B. Nichols, “Optimum Settings for Automatic Controllers,” *Journal of Fluids Engineering*, vol. 64, no. 8, pp. 759–765, 1942, doi: 10.1115/1.4019264.
[16] K. L. Chien, J. A. Hrones, and J. B. Reswick, “On the Automatic Control of Generalized Passive Systems,” *Journal of Fluids Engineering*, vol. 74, no. 2, pp. 175–183, 1952, doi: 10.1115/1.4015724.
[17] *Virtual Reality*. Washington, D.C.: National Academies Press, 1995.

CONTACTS

Max Jäger, M.Sc. email: max.jaeger@tu-ilmenau.de
ORCID: https://orcid.org/0000-0003-2203-4140
Dipl.-Ing. Thomas Helbig email: Thomas.helbig@tu-ilmenau.de
ORCID: https://orcid.org/0000-0002-3909-3078
Univ.-Prof. Dipl.-Ing. Dr. med. (habil.) H. Witte email: hartmut.witte@tu-ilmenau.de
ORCID: https://orcid.org/0000-0001-6055-2921

